Research Article Vol. 8, No. 6 / June 2021 / Optica 765

optica

Electron dynamics in laser-driven atoms near the continuum threshold

Mingqing Liu,[1,†] Songpo Xu,[2,3,†] Shilin Hu,[4] Wilhelm Becker,[5,6] Wei Quan,[2,3,8] Xiaojun Liu,[2,3,9] and Jing Chen[1,7,10]

[1]Institute of Applied Physics and Computational Mathematics, Beijing 100088, China
[2]State Key Laboratory of Magnetic Resonance and Atomic and Molecular Physics, Wuhan Institute of Physics and Mathematics, Innovation Academy for Precision Measurement Science and Technology, Chinese Academy of Sciences, Wuhan 430071, China
[3]University of Chinese Academy of Sciences, Beijing 100049, China
[4]Guangdong Provincial Key Laboratory of Quantum Metrology and Sensing & School of Physics and Astronomy, Sun Yat-Sen University (Zhuhai Campus), Zhuhai 519082, China
[5]Max-Born-Institut, Max-Born-Strasse 2a, 12489 Berlin, Germany
[6]National Research Nuclear University MEPhI, Kashirskoe Shosse 31, 115409 Moscow, Russia
[7]Shenzhen Key Laboratory of Ultraintense Laser and Advanced Material Technology, Center for Advanced Material Diagnostic Technology, and College of Engineering Physics, Shenzhen Technology University, Shenzhen 518118, China
[8]e-mail: charlywing@wipm.ac.cn
[9]e-mail: xjliu@wipm.ac.cn
[10]e-mail: chen_jing@iapcm.ac.cn

Received 4 January 2021; revised 4 April 2021; accepted 17 April 2021 (Doc. ID 418636); published 24 May 2021

Strong-field ionization and Rydberg-state excitation (RSE) near the continuum threshold exhibit two phenomena that have attracted a lot of recent attention: the low-energy structure (LES) just above and frustrated tunneling ionization just below the threshold. The former becomes apparent for longer laser wavelengths, while the latter has been especially investigated in the near infrared; both have been treated as separate phenomena so far. Here we present a unified perspective based on electron trajectories, which emphasizes the very important role of the electron-ion Coulomb interaction as expected in this energy region. Namely, those trajectories that generate the LES can also be recaptured into a Rydberg state. The coherent superposition of the contributions of such trajectories with different travel times (each generating one of the various LES peaks) causes an oscillation in the intensity dependence of the RSE yield, which is especially noticeable for longer wavelengths. The theory is illustrated by RSE experiments at 1800 nm, which agree very well with the theory with respect to position and period of the oscillation. The wavelength scaling of the RSE oscillation is also discussed. Our work establishes a solid relationship between processes below and above the threshold and sheds new light on atomic dynamics driven by intense laser fields in this critical energy region.

https://doi.org/10.1364/OPTICA.418636

1. INTRODUCTION

Thirty years after its discovery by Agostini *et al.* [1], above-threshold ionization (ATI) was considered to be well understood, when unexpectedly a peculiar low-energy structure (LES) was observed in the photoelectron energy spectrum [2,3]. Referred to as an "ionization surprise" [4], in fact, its appearance and explanation can be traced back to the double-hump structure observed in the longitudinal photoelectron momentum distribution of [5–7]. On the other hand, at about the same time the effect of highly excited bound (Rydberg) states in an intense laser field was revisited. The observed surprisingly strong survival of electrons in such states was dubbed "frustrated tunneling ionization" (FTI) [8–10]. Manifestation of Rydberg states in the spectra of the liberated electrons had been first observed by Freeman *et al*. in 1987 [11] and discussed mostly in the multiphoton resonance picture (later denoted "Freeman resonances"). Rydberg states were found also to be responsible for a substructure of the high-order ATI peaks [12]. In a seminal paper, trapping of significant populations in excited states had been deduced already from the electron spectra in a pump-probe experiment [13].

Enormous theoretical efforts have been made to explore the mechanisms underlying these phenomena near the threshold. Semiclassical models (by which we mean quantum-mechanical injection into the continuum followed by classical propagation of the liberated electron in the field) have come to play an essential role in explaining strong-field phenomena, emphasizing the general importance of the Coulomb-focusing mechanism [14,15], and have been applied to the study of the LES [3,16–19]. Full quantum-mechanical approaches include a Coulomb-corrected strong-field approximation (CCSFA) [20] and an improved SFA with or without consideration of the Coulomb potential [19,21]. It has become widely accepted that the Coulomb potential is

responsible for making the LES observable, via Coulomb focusing [3,16,17] and bunching of the photoelectron energy distribution caused by soft recollisions [5,17,18,22]. Meanwhile, ionization into very-low-energy states has displayed a rich variety of features in the angle-resolved spectrum, including in addition the very-low-energy structure (VLES), a zero-energy structure (ZES), or near-zero-energy structures, and a V structure [3,23–27]. Thus far, not all of them have found generally accepted explanations.

The semiclassical picture originated by the seminal work of Keldysh [28] is well suited to describe FTI [29] or the recapture of a tunneled electron by the ionic long-range Coulomb potential [8]. In spite of some controversy in the literature so far, this explains the experimental observations [9,30–33] reasonably well. The peaks in the intensity dependence of the Rydberg-state population, which are observed in time-dependent Schrödinger equation (TDSE) simulations and experiments, can be well understood as a channel-closing effect [34–38]. Apparently, they are beyond a semiclassical perspective. However, a recently developed quantum model shows that this peak structure can be attributed to the interference of electron wave packets released in different half-cycles of the laser pulse, and Rydberg-state excitation (RSE) occurs via a coherent recapture process [38,39].

Both the LES and FTI concern states around the continuum threshold and are closely related to the interaction between the tunneled electron and the ionic Coulomb potential. Hence, the relationship between these two processes is a very intriguing problem. However, the relevant physics are obscured partially by the fact that the LES is apparent for a mid-infrared laser field but difficult to observe at near-infrared wavelengths such as 800 nm [3,17]. On the other hand, this is the wavelength regime mostly adopted in the study of FTI [9,30]. Theoretically, Piraux *et al.* calculated RSE in a 1800-nm laser field via the TDSE and found an oscillatory structure in the intensity dependence of the Rydberg-state population with a period of about 50 TW/cm^2 [37]. This is clearly not consistent with the prediction by the channel-closing effect, which is 2.2 TW/cm^2. Rather, it was speculated to be due to a Raman process [37]. Unfortunately, it is hard to extract a clear physical picture from the TDSE calculation. However, this oscillatory structure is certainly beyond the scope of the semiclassical perspective, which due to its classical nature can only give a smooth intensity dependence irrespective of the wavelength. Therefore, a quantum model, which takes into account the interaction between the electron and the ionic potential, and an experiment performed at long wavelength are highly desirable for a full understanding of the relevant physics.

In this work, we present a joint theoretical and experimental study of RSE in an infrared intense laser field. We propose a quantum model that treats RSE as a coherent recapture process and includes the interaction between the electron and the ionic Coulomb potential. The calculation well reproduces the experimental and the TDSE results, which show an oscillatory structure with a period of $\Delta I \sim 50$ TW/cm^2 in the intensity dependence of the Rydberg-state population. Our analysis builds on the fact that forward scattering of the electron upon the ionic Coulomb potential when it returns to the core at different return times affects the electron trajectories and generates the LES. In addition, these electrons can be coherently captured by the Rydberg states, and interference between the contributions of trajectories of different returns gives rise to the observed oscillatory structure. Moreover, the wavelength dependence of the oscillation period is calculated. It is found to scale with $\lambda^{-1.2}$. For short wavelengths such as 800 nm, this period is too long to be observable. Atomic units ($\hbar = m_e = |e| = 1$) are used throughout unless otherwise specified.

2. METHODS

The RSE capture probability with the electron initially in the state $|\Psi_i\rangle$ is given by $P = \sum_{nlm} |M_{nlm}|^2$, and with $|M_{nlm}|$ it can be written by [39]

$$M_{nlm} = \lim_{t\to\infty} (-i)^2 \int_{-\infty}^{t} \mathrm{d}\tau' \int_{-\infty}^{\tau'} \mathrm{d}\tau \langle \Psi_{nlm}(t)| U(t,\tau') V \times U_V(\tau',\tau) H_I(\tau)|\Psi_i(\tau)\rangle, \tag{1}$$

where $U(t,\tau')$ denotes the total time-evolution operator with the Coulomb and the laser fields, and $U_V(\tau',\tau) = \int \mathrm{d}^3\boldsymbol{p} |\Psi_{\boldsymbol{p}}^{(V)}(\tau')\rangle\langle\Psi_{\boldsymbol{p}}^{(V)}(\tau)|$ denotes the Volkov time-evolution operator, which can be expanded in terms of the Volkov states $|\Psi_{\boldsymbol{p}}^{(V)}\rangle$. The operator H_I represents the interaction between the electron and the laser field, and V denotes the Coulomb potential. We attempt to take rescattering into account with the help of the Dyson equation

$$U(t,\tau') = U_V(t,\tau') - i\int_{\tau'}^{t} \mathrm{d}\tau'' U(t,\tau'') V U_V(\tau'',\tau'). \tag{2}$$

We have

$$M_{nlm} = \lim_{t\to\infty} (-i)^2 \int_{-\infty}^{t} \mathrm{d}\tau' \int_{-\infty}^{\tau'} \mathrm{d}\tau \langle \Psi_{nlm}(t) \times U_V(t,\tau') V U_V(\tau',\tau) H_I(\tau)\Psi_i(\tau)\rangle \tag{3}$$

$$+ \lim_{t\to\infty} (-i)^3 \int_{-\infty}^{t} \mathrm{d}\tau' \int_{-\infty}^{\tau'} \mathrm{d}\tau \int_{\tau'}^{t} \mathrm{d}\tau'' \langle \Psi_{nlm}(t)| U(t,\tau'') \times V U_V(\tau'',\tau') V U_V(\tau',\tau) H_I(\tau)|\Psi_i(\tau)\rangle. \tag{4}$$

The first term [Eq. (3)], which is linear in the Coulomb potential, does not contribute in the limit where $t\to\infty$, owing to the decreasing overlap between the localized Rydberg state and the spreading continuum wave function (see Supplement 1 for details). As shown in Ref. [39], the final state $\langle\Psi_{nlm}(t)|U(t,\tau'')$ can be approximated by the field-dressed Rydberg state

$$\Psi_{nlm}^{d}(\boldsymbol{r},\tau'') = \psi_{nlm}(\boldsymbol{r}) e^{-iE_n\tau''} e^{i\boldsymbol{r}\cdot\boldsymbol{A}(\tau'')} e^{-i\int_{-\infty}^{\tau''} \mathrm{d}\tau A^2(\tau)/2}, \tag{5}$$

which approximately satisfies the TDSE. The state $\psi_{nlm}(\boldsymbol{r})$ is a field-free Rydberg state corresponding to the energy level $E_n = -Z/(2n^2)$, and the principal, angular-momentum, and magnetic quantum numbers are n, l, and m, respectively. Hence, we obtain

$$\begin{aligned} M_{nlm} &= (-i)^3 \int_{-\infty}^{\infty} \mathrm{d}\tau' \int_{-\infty}^{\tau'} \mathrm{d}\tau \int_{\tau'}^{\infty} \mathrm{d}\tau'' \int \mathrm{d}^3\boldsymbol{p} \int \mathrm{d}^3\boldsymbol{k} \langle \Psi_{nlm}^{d}(\tau'')| V |\Psi_{\boldsymbol{p}}^{(V)}(\tau'')\rangle\langle\Psi_{\boldsymbol{p}}^{(V)}(\tau')| V |\Psi_{\boldsymbol{k}}^{(V)}(\tau')\rangle\langle\Psi_{\boldsymbol{k}}^{(V)}(\tau)| H_I |\Psi_i(\tau)\rangle \\ &= \frac{(-i)^3}{(2\pi)^6} \int_{-\infty}^{\infty} \mathrm{d}t_r \int_{-\infty}^{t_r} \mathrm{d}t_i \int_{t_r}^{\infty} \mathrm{d}t_c \int \mathrm{d}^3\boldsymbol{p} \int \mathrm{d}^3\boldsymbol{k} \langle \psi_{nlm}(\boldsymbol{r}_1)| -\frac{Z}{|\boldsymbol{r}_1|} |e^{i\boldsymbol{p}\cdot\boldsymbol{r}_1}\rangle\langle e^{-i\boldsymbol{p}\cdot\boldsymbol{r}_2}| - \frac{Z}{|\boldsymbol{r}_2|} |e^{i\boldsymbol{k}\cdot\boldsymbol{r}_2}\rangle\langle e^{-i[\boldsymbol{k}+\boldsymbol{A}(t_i)]\cdot\boldsymbol{r}_3} |\boldsymbol{r}_3\cdot\boldsymbol{E}(t_i)|\psi_i(\boldsymbol{r}_3)\rangle e^{iS(\boldsymbol{p},\boldsymbol{k},t_i,t_r,t_c)} \end{aligned} \tag{6}$$

with the action

$$S(\boldsymbol{p}, \boldsymbol{k}, t_i, t_r, t_c) = \frac{1}{2}\int_{-\infty}^{t_c} \mathrm{d}t \boldsymbol{A}^2(t) + E_n t_c - \frac{1}{2}\int_{t_r}^{t_c} \mathrm{d}t[\boldsymbol{p} + \boldsymbol{A}(t)]^2 - \frac{1}{2}\int_{t_i}^{t_r} \mathrm{d}t[\boldsymbol{k} + \boldsymbol{A}(t)]^2 + I_p t_i. \quad (7)$$

Clearly, times t_i, t_r, and t_c denote the instants of ionization, rescattering, and capture. $\boldsymbol{p}$ and $\boldsymbol{k}$ are the momenta after and before rescattering, respectively. The initial state $\psi_i(\boldsymbol{r})$ is described by a $3p_z$ Slater-type orbital of the Ar atom, and $Z = 1$. The linearly polarized electric field is $\boldsymbol{E}(t) = E_0 \sin \omega t\, \hat{\boldsymbol{e}}_z$ with the vector potential $\boldsymbol{A}(t) = -\int_{-\infty}^{t} \boldsymbol{E}(\tau)\mathrm{d}\tau$, where E_0 is the peak amplitude and $\hat{\boldsymbol{e}}_z$ a unit polarization vector. I_p is the ionization energy of the Ar atom. Note that in an earlier paper, where we studied RSE-yield oscillations in the near infrared (800 nm wavelength), the first-order expansion [Eq. (1)] with the replacement $\langle \Psi_{nlm}(t) U(t, \tau')| \rightarrow \langle \Psi_{nlm}(\tau')|$ was sufficient to generate the oscillations in the RSE yield [39]. In the present case, for the 1800 nm wavelength, the lowest-order term that accomplishes this is the second-order term. This is a clear indication that the responsible mechanisms are essentially different in the two wavelength regimes, for the near IR (800 nm) and the IR (1800 nm). Details of the derivation and calculation of Eq. (6) can be found in Supplement 1.

3. RESULTS

Figure 1(a) shows the RSE probability of an Ar atom as a function of the peak intensity for a 10-cycle linearly polarized pulse with a wavelength of 1800 nm (frequency $\omega = 0.0253$ a.u.) calculated from the quantum model Eq. (6) with the action Eq. (7). The RSE probability exhibits a pronounced oscillation structure with a period of about 50 TW cm^{-2}, in good agreement with the TDSE calculation [37].

For comparison, in Fig. 1(b) we present the measured intensity dependence of the yield of Ar* at 1800 nm. In our experiments, the 1800 nm femtosecond laser beam with 55-fs pulse duration is generated from an optical parametric amplifier pumped by a commercial Ti:sapphire laser system with a repetition rate of 1 kHz. A collimated supersonic beam of Ar atoms intersects the laser beam at the focal spot inside the vacuum chamber of a homemade velocity map imaging (VMI) spectrometer. The excited Ar atoms (with principal quantum numbers $n \leq 75$) produced by the laser field are detected by a position-sensitive microchannel plate (MCP) detector. With several special experimental efforts, the laser-intensity fluctuation can be controlled to be around 1.7%, and the laser intensity is determined via the $10U_p$ cutoff of the high-order above-threshold ionization photoelectron spectrum during the measurements (see Ref. [38] and Supplement 1). After focal averaging (for more details see Appendix of Ref. [38] and Supplement 1), the calculated intensity-dependent ratios of the focal-averaged excitation rate to the ionization rate are in good agreement with the experimental observation, including the positions of the minima and the oscillation period. The distinction between two curves in the high-intensity regime can be attributed to saturation of the detection efficiency of the MCP detector (see Supplement 1 for details), which is not taken into account in the calculation. Our result is also well consistent with the TDSE calculation of Ref. [37].

To shed more light on the physical mechanism underlying RSE at long wavelengths, we calculate the n-distribution of the RSE probability for several typical intensities between 200 and 250 TW/cm^2 as shown in Fig. 2(a). We see that the excitation yield increases when the intensity increases from 200 to 230 TW/cm^2 and decreases between 230 and 250 TW/cm^2. However, the populations of the Rydberg states with $n = 9$ stay dominant in the whole intensity regime, in agreement with our previous prediction $n \sim E_0^{1/2}/\omega$ [39]. Therefore, for the sake of simplicity, we choose the final Rydberg state [0,8,9] ($n = 9$, $l = 8$, $m = 0$) to illustrate the recapture picture in the following analysis. The calculated excitation probability of the state [0,8,9] is presented in Fig. 2(b), which shows an oscillation structure very similar to that of the total RSE with respect to period and positions of the minima and maxima. In addition, we display the result of the quantum model earlier proposed in Ref. [39] {refer to Eq. (15) of Ref. [39]}. This model differs from Eq. (6) by not accounting for the scattering event preceding the recapture. It yields a smooth curve after performing the three-dimensional focal average [36], which smears out the fast oscillation (with a period of 2.2 TW/cm^2) due to the channel-closing effect, indicating that the interaction between the electron and the ion is instrumental for the formation of the oscillations of the RSE probability—the same interaction that also generates the LES.

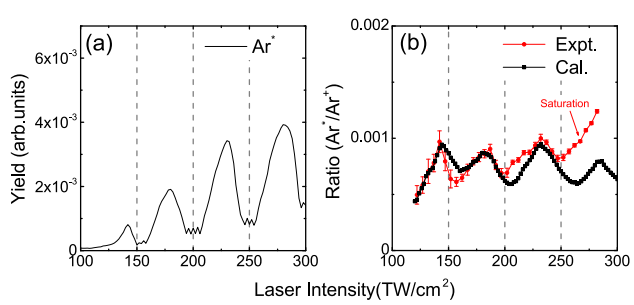

Fig. 1. (a) Calculated intensity dependence of the excitation probability of an argon atom exposed to a 10-cycle 1800-nm laser pulse without focal averaging. The principal quantum number is in the range of $4 \leq n \leq 20$. (b) The ratio of the focal-averaged result of panel (a) to the ionization rate calculated by the SFA theory and by the experimental measurement.

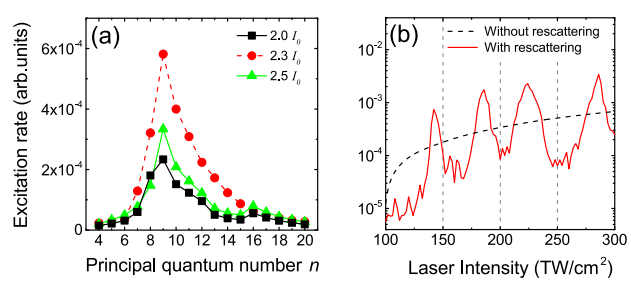

Fig. 2. (a) Distribution of the principal quantum number n of the RSE for Ar for three intensities ($I_0 = 10^{14}$ W/cm^2). (b) Calculated excitation rate as a function of the laser intensity for the Rydberg state of [0, 8, 9] by using Eq. (15) in Ref. [39] (black dashed line) and Eq. (6) in the text (red solid line).

4. DISCUSSION

To further explore the mechanism of the oscillation structure and, especially, its close connection with the electron-ion interaction, in Fig. 3(a) we exhibit typical electron trajectories (after ionization, in the presence of only the laser field) for an intensity of 200 TW/cm^2, for several drift energies as indicated. It is worthwhile mentioning that we do not take into account the tunneling exit in the analysis since, compared with the quiver amplitude of the electron (over 100 a.u.), the influence of the tunneling exit (less than 10 a.u.) is negligible. The LES peaks are generated by trajectories that turn around (so that their velocity goes through zero) at the position of the ion, i.e., at $z = 0$ [19]. The electron can be recaptured by a Rydberg state if its trajectory turns around within the spatial range where this state is concentrated, indicated for $n = 9$, $l = 8$, $m = 0$ by the two horizontal orange stripes in Fig. 3(a). The trajectory corresponding to the first LES peak ($\mu = 1$ in the notation of Ref. [19]) and the energy $0.09U_p$ [red solid line in Fig. 3(a)] cannot be recaptured, but trajectories for lower energies can. For example, the trajectory (red dashed line) with a drift energy of $0.05U_p$ can be recaptured around $t = 1.7T$ in the capture region of $z < 0$ or around $t = 2.7T$ in the capture region of $z > 0$ having been forward scattered at about $t = 1.6T$ or $t = 1.9T$. The (light-blue) trajectory with its drift energy of $0.032U_p$ corresponds to the second LES peak ($\mu = 2$). It can only be recaptured in the $z > 0$ region at around $t = 3.7T$. Figure 3(b) displays the drift-energy ranges that allow for recapture extracted from these trajectory calculations.

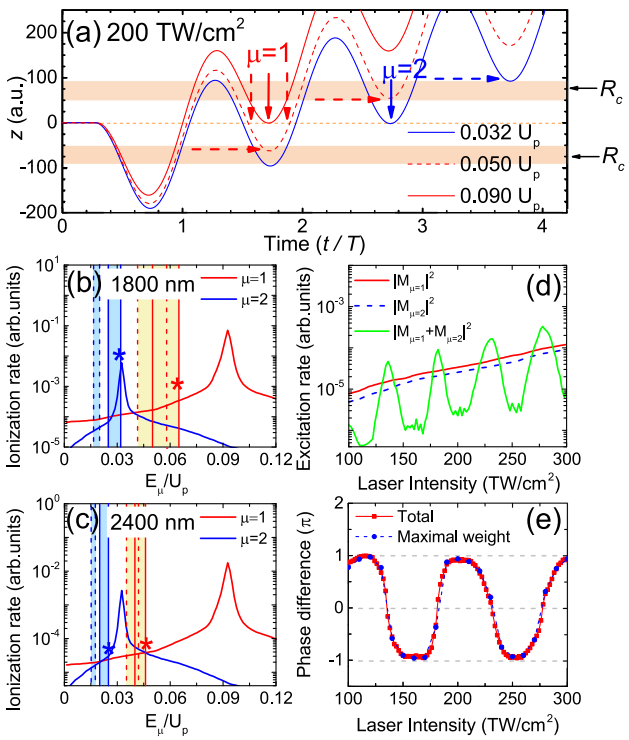

Fig. 3. (a) Typical simple-man trajectories with different final kinetic energies (given in multiples of U_p) corresponding to $\mu = 1$ and $\mu = 2$ for 200 TW/cm^2 and $\lambda = 1800$ nm. Actually, the various trajectories start at very slightly different times, but this is not visible on the scale of the figure. The two horizontal orange stripes denote the spatial capture regions for positive and negative z as introduced by Fig. S1(a) in Supplement 1. The vertical and horizontal arrows indicate the return times t_r and capture times t_c, respectively, for $\mu = 1$ and $\mu = 2$. (b) The LES energy spectra of $\mu = 1$ and $\mu = 2$ for 200 TW/cm^2 and $\lambda = 1800$ nm nm (solid curves). The shaded regions in between the vertical solid (the vertical dashed) lines represent the energy ranges of capture according to panel (a) for positive (negative) z. (c) The same as panel (b) except that the wavelength is 2400 nm. (d) Calculated intensity dependence of the RSE probabilities corresponding to $\mu = 1$ and $\mu = 2$ as well as their coherent sum at 1800 nm. (e) Intensity dependence of the phase difference between the RSE amplitudes for $\mu = 1$ and $\mu = 2$, and that between two trajectories with the maximal weights for each μ. See text and Supplement 1 for more details.

The RSE yields for $\mu = 1$ and $\mu = 2$ are separately exhibited in Fig. 3(d). Both curves are smooth and display no oscillatory structure. However, their coherent superposition does show an oscillation with a period of about 50 TW/cm^2, in agreement with the result of Fig. 2(b), implying that it is the interference between the RSE amplitudes corresponding to $\mu = 1$ and $\mu = 2$ that is responsible for the oscillation structure observed in the total RSE yield [40]. This can be confirmed by looking at Fig. 3(e), which shows that the phase difference between the two trajectories changes periodically between $-\pi$ and π with increasing intensity, corresponding to the oscillation shown in Fig. 3(d). In addition, the phase difference between the RSE amplitudes corresponding to $\mu = 1$ and $\mu = 2$ can be approximately calculated by only considering the phase difference between the two trajectories with the maximal weights for each μ. Their energies are $0.065U_p$ and $0.032U_p$ for $\mu = 1$ and $\mu = 2$, respectively, for the parameters of Fig. 3(b) [indicated by the asterisks in Fig. 3(b)]. As shown in Fig. 3(e), the calculated phase difference using these two most important trajectories is indeed well consistent with the complete calculation. The above analysis hinges on the fact that forward scattering was taken into account, which is responsible for both the LES peaks and the oscillations. Nevertheless, trajectories in the entire energy range contribute to the interference via their smooth energy spectrum and hence smear out the oscillation structures. It is worthwhile to mention that so far only forward scattering, i.e., $\boldsymbol{p} = \boldsymbol{k}$ in Eq. (6), is considered in our calculation. If the momentum of the electron is allowed to change during the collision, the RSE probability will be enhanced due to the Coulomb focusing effect [14,15]. However, it will not change the main result of this paper.

An interesting question that remains is how the oscillation structure depends on the wavelength of the laser field. To answer this question, we calculate the RSE probabilities of Ar for different wavelengths and present the results in Fig. 4(a). One can see that with increasing wavelength the period of the oscillation decreases. This is because the energy range of the electrons that contributes to RSE shrinks and shifts to lower energies with increasing laser wavelength as can be seen by comparing Fig. 3(c) with Fig. 3(b). The oscillation period extracted from our calculation shows

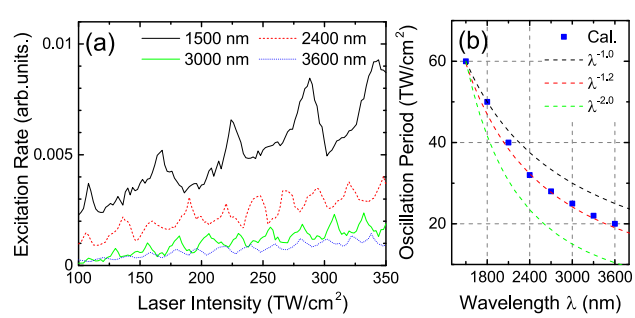

Fig. 4. (a) Intensity dependence of the RSE probability calculated by the quantum model for different laser wavelengths. (b) Wavelength dependence of the oscillation period of the calculated RSE probability.

a wavelength scaling of $\lambda^{-1.2}$ as depicted in Fig. 4(b) (see Supplement 1 for a more detailed analysis). According to this scaling law, the oscillation period for 800 nm would be larger than 130 $\mathrm{TW/cm^2}$. However, for 800 nm there are also oscillations in the RSE intensity dependence with a period of 26 $\mathrm{TW/cm^2}$, which are due to the channel-closing effect [34,36,37,39]. It is hardly possible to distinguish such a slow oscillation on a fast-oscillation background.

5. CONCLUSION

In conclusion, theoretically and experimentally we studied Rydberg-state excitation of an Ar atom exposed to an intense long-wavelength laser pulse. The RSE probability calculated with a quantum model that takes into account the soft collision between the electron and the Coulomb potential is well consistent with a TDSE calculation and the experimental observations, showing for a wavelength of 1800 nm an oscillation with a period $\Delta I \sim 50\ \mathrm{TW/cm^2}$ in the intensity dependence of the Rydberg-state population. This oscillation and its period result from interference between trajectories in which the electrons undergo forward scattering off the ionic Coulomb potential at different return times before being captured by the Rydberg state. Forward scattering after different travel times is also responsible for the generation of the series of LES peaks. In addition, the wavelength scaling of the oscillation period was discussed and found to be $\lambda^{-1.2}$. Our work establishes a straight relationship between the LES and the RSE processes, unifying the physics ongoing in this critical energy region below and above the continuum threshold and providing a new perspective of its very rich phenomenology.

Funding. National Key Research and Development Program of China (2019YFA0307700, 2016YFA0401100); National Natural Science Foundation of China (11527807, 11774387, 11804405, 11834015, 11974383); Department of Science and Technology, Hubei Provincial People's Government (2019CFA035, 2020CFA029); Strategic Priority Research Program of the Chinese Academy of Sciences (XDB21010400).

Disclosures. The authors declare no conflicts of interest.

Data Availability. Data underlying the results presented in this paper are not publicly available at this time but may be obtained from the authors upon reasonable request.

Supplemental document. See Supplement 1 for supporting content.

†These authors contributed equally to this work.

REFERENCES AND NOTE

1. P. Agostini, F. Fabre, G. Mainfray, G. Petite, and N. K. Rahman, "Free-free transitions following six-photon ionization of xenon atoms," Phys. Rev. Lett. **42**, 1127–1130 (1979).
2. C. I. Blaga, F. Catoire, P. Colosimo, G. G. Paulus, H. G. Muller, P. Agostini, and L. F. DiMauro, "Strong-field photoionization revisited," Nat. Phys. **5**, 335–338 (2009).
3. W. Quan, Z. Lin, M. Wu, H. Kang, H. Liu, X. Liu, J. Chen, J. Liu, X. T. He, S. G. Chen, H. Xiong, L. Guo, H. Xu, Y. Fu, Y. Cheng, and Z. Z. Xu, "Classical aspects in above-threshold ionization with a midinfrared strong laser field," Phys. Rev. Lett. **103**, 093001 (2009).
4. F. H. M. Faisal, "Strong-field physics: ionization surprise," Nat. Phys. **5**, 319–320 (2009).
5. J. Chen and C. H. Nam, "Ion momentum distributions for He single and double ionization in strong laser fields," Phys. Rev. A **66**, 053415 (2002).
6. R. Moshammer, J. Ullrich, B. Feuerstein, D. Fischer, A. Dorn, C. D. Schröter, J. R. Crespo Lopez-Urrutia, C. Hoehr, H. Rottke, C. Trump, M. Wittmann, G. Korn, and W. Sandner, "Rescattering of ultralow-energy electrons for single ionization of Ne in the tunneling regime," Phys. Rev. Lett. **91**, 113002 (2003).
7. L. Guo, J. Chen, J. Liu, and Y. Q. Gu, "Origin of the double-peak structure in longitudinal momentum distribution for single ionization of an He atom in strong laser field," Phys. Rev. A **66**, 053415 (2008).
8. B. B. Wang, X. F. Li, P. M. Fu, J. Chen, and J. Liu, "Coulomb potential recapture effect in above-barrier ionization in laser pulse," Chin. Phys. Lett. **23**, 2729–2732 (2006).
9. T. Nubbemeyer, K. Gorling, A. Saenz, U. Eichmann, and W. Sandner, "Strong-field tunneling without ionization," Phys. Rev. Lett. **101**, 233001 (2008).
10. N. I. Shvetsov-Shilovski, S. P. Goreslavski, S. V. Popruzhenko, and W. Becker, "Capture into Rydberg states and momentum distributions of ionized electrons," Laser Phys. **19**, 1550–1558 (2009).
11. R. R. Freeman, P. H. Bucksbaum, H. Milchberg, S. Darack, D. Schumacher, and M. E. Geusic, "Above-threshold ionization with subpicosecond laser pulses," Phys. Rev. Lett. **59**, 1092–1095 (1987).
12. M. J. Nandor, M. A. Walker, L. D. Van Woerkom, and H. G. Muller, "Detailed comparison of above-threshold-ionization spectra from accurate numerical integrations and high-resolution measurements," Phys. Rev. A **60**, R1771–R1774 (1999).
13. M. P. de Boer and H. G. Muller, "Observation of large populations in excited states after short-pulse multiphoton ionization," Phys. Rev. Lett. **68**, 2747–2750 (1992).
14. T. Brabec, M. Yu. Ivanov, and P. B. Corkum, "Coulomb focusing in intense field atomic processes," Phys. Rev. A **54**, R2551–R2554 (1996).
15. G. L. Yudin and M. Yu. Ivanov, "Physics of correlated double ionization of atoms in intense laser fields: quasistatic tunneling limit," Phys. Rev. A **63**, 033404 (2001).
16. C. P. Liu and K. Z. Hatsagortsyan, "Origin of unexpected low energy structure in photoelectron spectra induced by midinfrared strong laser fields," Phys. Rev. Lett. **105**, 113003 (2010).
17. C. Y. Wu, Y. D. Yang, Y. Q. Liu, Q. H. Gong, M. Y. Wu, X. Liu, X. L. Hao, W. D. Li, X. T. He, and J. Chen, "Characteristic spectrum of very low-energy photoelectron from above-threshold ionization in the tunneling regime," Phys. Rev. Lett. **109**, 043001 (2012).
18. A. Kästner, U. Saalmann, and J. M. Rost, "Electron-energy bunching in laser-driven soft recollisions," Phys. Rev. Lett. **108**, 033201 (2012).
19. W. Becker, S. P. Goreslavski, D. B. Milošević, and G. G. Paulus, "Low-energy electron rescattering in laser-induced ionization," J. Phys. B **47**, 204022 (2014).
20. T. Yan, S. V. Popruzhenko, M. J. J. Vrakking, and D. Bauer, "Low-energy structures in strong field ionization revealed by quantum orbits," Phys. Rev. Lett. **105**, 253002 (2010).
21. L. Guo, S. S. Han, X. Liu, Y. Cheng, Z. Z. Xu, J. Fan, J. Chen, S. G. Chen, W. Becker, C. I. Blaga, A. D. DiChiara, E. Sistrunk, P. Agostini, and L. F. DiMauro, "Scaling of the low-energy structure in above-threshold ionization in the tunneling regime: theory and experiment," Phys. Rev. Lett. **110**, 013001 (2013).
22. S. A. Kelvich, W. Becker, and S. P. Goreslavski, "Coulomb focusing and defocusing in above-threshold ionization spectra produced by strong mid-IR laser pulses," Phys. Rev. A **93**, 033411 (2016).
23. J. Dura, N. Camus, A. Thai, A. Britz, M. Hemmer, M. Baudisch, A. Senftleben, C. D. Schröter, J. Ullrich, R. Moshammer, and J. Biegert, "Ionization with low-frequency fields in the tunneling regime," Sci. Rep. **3**, 2675 (2013).
24. M. G. Pullen, J. Dura, B. Wolter, M. Baudisch, M. Hemmer, N. Camus, A. Senftleben, C. D. Schroeter, R. Moshammer, J. Ullrich, and J. Biegert, "Kinematically complete measurements of strong field ionization with mid-IR pulses," J. Phys. B **47**, 204010 (2014).
25. E. Diesen, U. Saalmann, M. Richter, M. Kunitski, R. Dörner, and J. M. Rost, "Dynamical characteristics of Rydberg electrons released by a weak electric field," Phys. Rev. Lett. **116**, 143006 (2016).
26. W. Becker and D. B. Milošević, "Above-threshold ionization for very low electron energy," J. Phys. B **48**, 151001 (2015).
27. E. Pisanty and M. Yu. Ivanov, "Kinematic origin for near-zero energy structures in mid-IR strong field ionization," J. Phys. B **49**, 105601 (2016).
28. L. V. Keldysh, "Ionization in the field of a strong electromagnetic wave," Sov. Phys. JETP **20**, 1307–1314 (1965).
29. S. V. Popruzhenko, "Quantum theory of strong-field frustrated tunneling," J. Phys. B **51**, 014002 (2018).

30. U. Eichmann, T. Nubbemeyer, H. Rottke, and W. Sandner, "Acceleration of neutral atoms in strong short-pulse laser fields," Nature **461**, 1261–1265 (2009).
31. T. Nubbemeyer, U. Eichmann, and W. Sandner, "Excited neutral atomic fragments in the strong-field dissociation of N_2 molecules," J. Phys. B **42**, 134010 (2009).
32. U. Eichmann, A. Saenz, S. Eilzer, T. Nubbemeyer, and W. Sandner, "Observing Rydberg atoms to survive intense laser fields," Phys. Rev. Lett. **110**, 203002 (2013).
33. H. Zimmermann, J. Buller, S. Eilzer, and U. Eichmann, "Strong-field excitation of helium: bound state distribution and spin effects," Phys. Rev. Lett. **114**, 123003 (2015).
34. Q. Li, X. M. Tong, T. Morishita, H. Wei, and C. D. Lin, "Fine structures in the intensity dependence of excitation and ionization probabilities of Hydrogen atoms in intense 800-nm laser pulses," Phys. Rev. A **89**, 023421 (2014).
35. A. M. Popov, O. V. Tikhonova, and E. A. Volkova, "Low frequency strong field ionization and excitation of Hydrogen atom," Laser Phys. **20**, 1028–1037 (2010).
36. H. Zimmermann, S. Patchkovskii, M. Ivanov, and U. Eichmann, "Unified time and frequency picture of ultrafast atomic excitation in strong laser fields," Phys. Rev. Lett. **118**, 013003 (2017).
37. B. Piraux, F. Mota-Furtado, P. F. O'Mahony, A. Galstyan, and Yu. V. Popov, "Excitation of Rydberg wave packets in the tunneling regime," Phys. Rev. A **96**, 043403 (2017).
38. S. P. Xu, M. Q. Liu, S. L. Hu, Z. Shu, W. Quan, Z. L. Xiao, Y. Zhou, M. Z. Wei, M. Zhao, R. P. Sun, Y. L. Wang, L. Q. Hua, C. Gong, X. Y. Lai, J. Chen, and X. J. Liu, "Observation of a transition in the dynamics of strong-field atomic excitation," Phys. Rev. A **102**, 043104 (2020).
39. S. L. Hu, X. L. Hao, H. Lv, M. Q. Liu, T. X. Yang, H. F. Xu, M. X. Jin, D. J. Ding, Q. G. Li, W. D. Li, W. Becker, and J. Chen, "Quantum dynamics of atomic Rydberg excitation in an intense laser field," Opt. Express **27**, 31629–31643 (2019).
40. Another example of an effect that can be explained by the coherent superposition of the contributions of several quantum orbits is given by the intensity-dependent enhancements in the ATI rescattering plateau; see G. G. Paulus, F. Grasbon, H. Walther, R. Kopold, and W. Becker, "Channel-closing-induced resonances in the above-threshold ionization plateau," Phys. Rev. A **64**, 021401 (2001).